# Convectively Coupled Kelvin Waves over Tropical Africa during the Boreal Summer: Structure and Variability

ADEME MEKONNEN AND CHRIS D. THORNCROFT

*Department of Earth and Atmospheric Sciences, University at Albany, State University of New York, Albany, New York*

ANANTHA R. AIYYER

*Department of Marine, Earth and Atmospheric Sciences, North Carolina State University, Raleigh, North Carolina*

GEORGE N. KILADIS

*NOAA/Earth Systems Research Laboratory, Boulder, Colorado*

(Manuscript received 23 April 2007, in final form 16 May 2008)

ABSTRACT

The structure and variability of convectively coupled Kelvin waves during the boreal summer are explored using satellite-observed brightness temperature data and ECMWF reanalyses. Kelvin wave activity is most prominent between the central and eastern Pacific, across Africa, and the Indian Ocean. Composite analysis shows that over sub-Saharan Africa Kelvin wave convection is peaked north of the equator, while the dynamical fields tend to be symmetric with respect to the equator. Convectively coupled Kelvin waves propagate faster over the Pacific and western Atlantic ($\sim$24 m s$^{-1}$), and slow down over tropical Africa ($\sim$14 m s$^{-1}$), consistent with stronger coupling between the dynamics and convection over tropical Africa. The Kelvin waves observed over Africa generally propagate into the region from anywhere between the eastern Pacific and the Atlantic, and decay over the eastern Indian Ocean basin.

Results show marked interannual variability of Kelvin wave activity over Africa. Anomalously high Kelvin wave variance tends to occur during dry years, while low variance occurs during wet years. African Kelvin wave activity is positively correlated with SST anomalies in the equatorial east Pacific. The same warm SST anomalies that are favorable for enhanced Kelvin wave activity suppress the mean rainfall over tropical Africa via a more slowly varying teleconnection and associated subsidence.

A brief analysis of an intense Kelvin wave in August 1987 (a dry year) shows a clear impact of the wave on convective development and daily rainfall over tropical Africa. This Kelvin wave was also associated with a series of easterly wave initiations over tropical Africa.

## 1. Introduction

A significant part of the synoptic-scale convective variability in the tropics is associated with equatorially trapped waves (e.g., Wheeler and Kiladis 1999, hereafter WK99). This includes Kelvin waves that are treated theoretically by Matsuno (1966) and confirmed by observational studies (e.g., Takayabu 1994; WK99). This study is concerned with investigating the nature and variability of convectively coupled Kelvin waves that impact convection and rainfall over tropical Africa during the boreal summer.

Tropical North Africa is dominated by westward-moving synoptic-scale African easterly waves (AEWs) during the northern summer monsoon season (e.g., Reed et al. 1977). In their study of the AEWs, Mekonnen et al. (2006) observed eastward-propagating convective features over this region, which are especially notable over central and eastern Africa. Mekonnen (2006) and Mounier et al. (2007, 2008) have recently shown evidence of convectively coupled Kelvin wave activity over the region based on satellite-observed brightness temperature, outgoing longwave radiation (OLR), and reanalysis datasets.

*Corresponding author address:* Ademe Mekonnen, Department of Earth and Atmospheric Sciences, University at Albany, State University of New York, 1400 Washington Ave., Albany, NY 12222-0001.
E-mail: ademe@atmos.albany.edu

DOI: 10.1175/2008JCLI2008.1

Several studies (e.g., Takayabu and Murakami 1991; Takayabu 1994), using satellite-observed cloud and kinematics data, have shown that eastward-moving "superclusters" over the west Pacific are often associated with Kelvin wave events during boreal summer. Convectively coupled synoptic-scale Kelvin waves typically have a zonal wavelength between 3000 and 6000 km and a phase speed between 15 and 25 m $s^{-1}$ (e.g., Wheeler et al. 2000, hereafter WKW00; Straub and Kiladis 2003a,b hereafter SK03a, SK03b, respectively). There has been considerable effort to study the impact of Kelvin waves on convection and rainfall over the Indian and Pacific basins.

In a case study that combined observations and European Centre for Medium-Range Weather Forecast (ECMWF) reanalysis, Straub and Kiladis (2002, hereafter SK02) showed that convective activity is enhanced as the Kelvin wave approaches the equatorial Pacific near the date line, while it weakens after the wave has passed. In their study of equatorial African convection during the boreal spring, Nguyen and Duvel (2008) also demonstrated a close connection between the synoptic time-scale convection and Kelvin wave activity. A similar study by Wang and Fu (2007) has examined the role of convectively coupled Kelvin waves during the boreal spring. Wang and Fu suggested that the anomalous precipitation over South America can impact the variability of the Atlantic intertropical convergence zone (ITCZ) via Kelvin waves that propagate between these regions.

Compared with other tropical regions, relatively little is known about Kelvin waves and their association with rainfall and convection over tropical Africa during the boreal summer. Mounier et al. (2007) showed that Kelvin waves modulate convection, including mesoscale convective systems (MCSs), over West Africa by enhancing the low-level westerly monsoon flow. They indicated that the interaction between Kelvin waves and convection is strong over West and central Africa. We will show that the Kelvin wave activity also has a strong impact over eastern Africa.

Several key research issues relevant to tropical Africa that have not been fully explored will be addressed in the present study. The specific objectives of this work are as follows:

(i) to explore the nature of convectively coupled Kelvin waves, including their impact on convection and rainfall over tropical Africa, and
(ii) to describe and interpret the interannual variability of the Kelvin wave activity over tropical North Africa.

The paper is organized as follows. Section 2 presents a brief description of the data and methodologies used. In section 3, we discuss the mean characteristics of convectively coupled Kelvin waves that affect sub-Saharan Africa during the boreal summer monsoon season. The source regions of these Kelvin waves and their initiation mechanisms are also briefly discussed in this section. Section 4 highlights the interannual variability of Kelvin wave activity and its relationship with near and remote sea surface temperature and rainfall variability. In section 5, a specific case study will be presented to highlight the impact of a Kelvin wave on convection and daily rainfall over tropical Africa. Finally, in section 6, major findings of the study are summarized.

## 2. Data and methodology

### *a. Data*

The characteristics of convection studied here are based on satellite-observed brightness temperature ($T_B$) data. These data are obtained from the Cloud Archive User Service (CLAUS) of the European Union. CLAUS $T_B$ is a product of multiple satellite observations (both geostationary and polar orbiting) in a 10–12-$\mu$m infrared window; it is a high-resolution dataset (3 hourly, global 0.5° × 0.5° grid). CLAUS $T_B$ is described in detail by Hodges et al. (2000). This dataset has been successfully applied to the study of the diurnal cycle by Yang and Slingo (2001) and to the study of AEWs and convection by Mekonnen et al. (2006). The period of record used here is from 1984 to 2004.

The kinematical and dynamical fields are based on reanalysis data obtained from the 40-yr ECMWF Re-Analysis (ERA-40). ERA-40 is a 6-hourly, 2.5° horizontal grid, and 23-pressure-level resolution dataset. The period of record that is used is 1984–2001. Although observational data that went into the reanalysis project is sparse over Africa, especially over the central and eastern parts, many past studies have shown that this dataset is adequate for the synoptic-scale analysis. As will be shown later, the analysis based on $T_B$ and ERA-40 reveal coherent convective and dynamical signals of propagating waves. The fact that these independent datasets show coherent results gives us confidence in the dynamical fields. This analysis system has also been evaluated by Tompkins et al. (2005) for the study of African easterly jet for a day in August 2000 and was found to be of good quality, despite sparse data.

Other datasets used include the following: (i) sea surface temperature (SST; monthly from 1984 to 2004, 1° horizontal resolution) from the Met Office Hadley Centre [i.e., Hadley Centre Global Sea Ice and Sea Surface Temperature (HADISST1); Rayner et al.

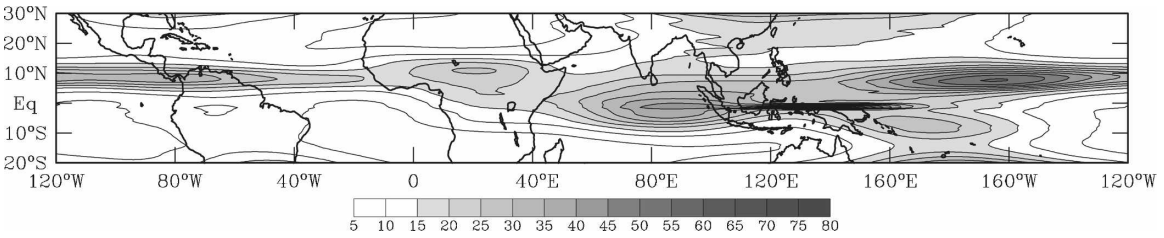


FIG. 1. The geographical distribution of Kelvin-filtered $T_B$ variance ($K^2$) for JAS 1984–2004.

2003]; (ii) observed rainfall from eight Ethiopian stations (daily from 1984 to 2004); and (iii) estimated rainfall (monthly from 1984 to 2004, 2.5° resolution) from the Climate Prediction Center (CPC) Merged Analysis Project (CMAP). These data are compiled by merging gauge observations, satellite estimates, and numerical model predictions (see Xie and Arkin 1997 for details). Additionally, (iv) rainfall data (daily from 1984 to 1990, 2.5° resolution) are obtained as well, from Institut de Recherches pour le Développment (IRD), France. These data are compiled based on observations of more than 860 stations and are available for the region 0°–25°N, 32.5°W–30°E.

### b. Methodology

Wavenumber–frequency filtering on the 21-yr $T_B$ time series has been carried out following the method of WK99. Details of the wavenumber–frequency filtering technique, its merits, and applications, are described in WK99 and WKW00. This method has also been successfully applied in other studies based on OLR (e.g., SK02; SK03a; SK03b), and on precipitable water data (Roundy and Frank 2004). Briefly, the method decomposes a data field into wavenumber–frequency components for eastward- and westward-moving wave types, and the resulting spectral density is plotted as a function of wavenumber and frequency (WK99, their Fig. 6). The decomposition is performed by using 96-day segments such that each segment overlaps the previous segment for 31 days. Prior to the decomposition, the data series is detrended and the ends of the time series were tapered to zero to control spectral leakage. WK99 have shown that overlapping of the time series does not affect results. This process identifies regions of a significant wavenumber–frequency domain for each wave type.

In this study, Kelvin wave filtering is performed within the period of 2.5–17 days, and eastward wavenumber 1–14, as in SK02. WK99 and WKW00 performed the filtering after decomposing data for symmetric and antisymmetric components of the OLR. However, here, the filtering is carried out on the total $T_B$, without separating the field into symmetric and antisymmetric components (SK02). The basis for this method is that the convective activity over tropical Africa and other tropical regions during the boreal summer is maximized well to the north of the equator, along the ITCZ. We will show that the eastward-moving convective activity is nearly symmetric about the mean location of the ITCZ, rather than the equator.

A linear regression technique has been applied to form composites of convectively coupled wave structures. As in WKW00, we first choose a base point (reference point) where wave-filtered $T_B$ variance is a maximum over the region of interest, and the time series at this point is derived from the Kelvin wave–filtered data. Then, a total field (e.g., unfiltered $T_B$, winds, geopotential height, and velocity potential) is regressed onto the reference time series at various time lags. The results are scaled for anomalies at $-1$ standard deviation of the base point–filtered $T_B$ time series to represent convective conditions at the base point. Correlations are tested for significance based on the two-tailed Student's $t$ test (see also WKW00).

## 3. Synoptic evolution of convectively coupled Kelvin waves affecting Africa

### a. Introduction

In this section, we present the mean synoptic structure of convectively coupled Kelvin waves that affect tropical Africa, including how they evolve from their source regions and propagate toward East Africa. Knowledge of the initiation regions may have implications for monitoring and prediction strategies and, thus, we briefly consider the source regions of Kelvin waves.

Figure 1 shows the mean geographical distribution of the Kelvin-filtered $T_B$ variance [averaged over 1984–2004 for July–September (JAS)]. Peak activity is seen around 10°N over tropical Africa, over the equatorial Indian Ocean, and along 5°–10°N over the western and central Pacific. The variance also stretches toward the eastern Pacific, Central America, and the Atlantic ITCZ. The Kelvin $T_B$ variance is not symmetric with respect to the equator, except over the Indian Ocean,

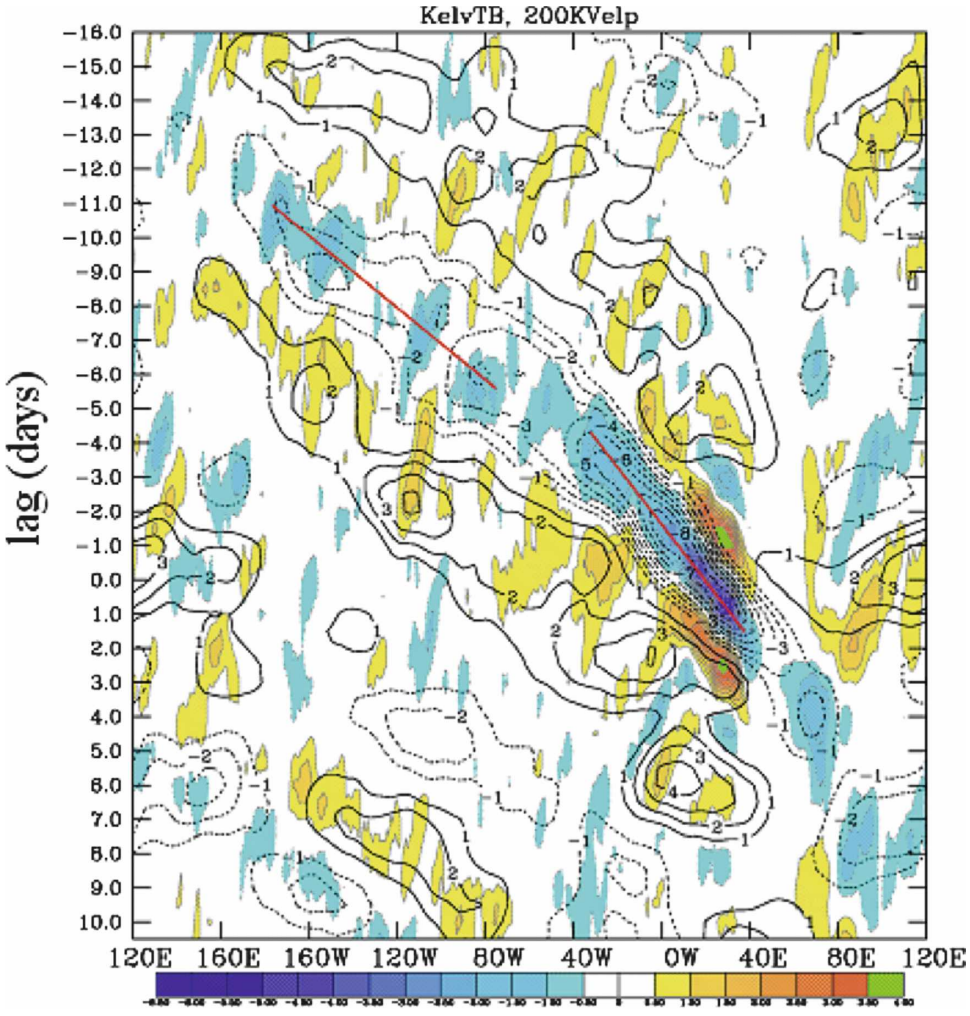


FIG. 2. Hovmöller diagram of 200-hPa velocity potential and total $T_B$ regressed onto Kelvin-filtered $T_B$ time series at 10°N, 20°E. Velocity potential anomalies are contoured every $1 \times 10^5$ m$^2$ s$^{-1}$ and $T_B$ anomalies are shaded every 0.5 K. Shown are latitudinal averages between 7° and 12°N. The red-colored slopes indicate an average speed of (top) 25 and (bottom) 14 m s$^{-1}$ over the Pacific–western Atlantic sector and tropical Africa, respectively.

consistent with previous analyses of Kelvin wave variance (e.g., SK02; Roundy and Frank 2004).

Although weaker compared with the central Pacific and Indian Ocean (with peak variance of ~50 K$^2$), Kelvin wave activity is clearly present over tropical Africa with a peak variance of ~25 K$^2$. We now apply a statistical linear regression technique to closely examine the mean synoptic structure of Kelvin waves based on convective and dynamical measures. Because the maximum Kelvin-filtered $T_B$ variance over tropical Africa during the boreal summer (July–September) is located near 10°N, 20°E, the Kelvin-filtered $T_B$ time series at this point is chosen as a base point (predictor), and, hence, unless specified, the composite analyses that follow are based on this point.

### b. *Mean synoptic structure*

Figure 2 is a Hovmöller diagram of unfiltered $T_B$ and 200-hPa velocity potential, both of which are projected onto the base point time series. The results are averaged in the 7°–12°N latitude belt, which is the region of peak Kelvin wave variance over Africa. The figure shows the $T_B$ signal associated with convectively coupled Kelvin waves that propagate from the Pacific toward eastern Africa. Convective and dynamical measures are in phase; enhanced convection is coincident with strong outflow and suppressed convection is aligned with upper-level convergence as inferred from the velocity potential. The strongest and most coherent Kelvin wave structures are seen between the central

Atlantic (near 40°W) and eastern Africa, although the results suggest that at least some of these waves start farther west over the central and eastern Pacific.

Further inspection of Fig. 2 indicates that the phase speed of the Kelvin wave changes as it propagates across different regions. The wave propagates faster over the central and eastern Pacific ($\sim$24 m s$^{-1}$),[1] and slows down over Africa ($\sim$14 m s$^{-1}$). The slowing down of the wave is suggestive of stronger coupling between the dynamical and convective signatures (cf. WKW00). It is also observed that the wave periodicity decreases from about 8 days over the Pacific and the Atlantic to about 4 days over central and eastern Africa. Consistent with this, the zonal scale of the wave contracts as it propagates eastward, changing from about 7000 km in the Pacific–Atlantic basin to about 5000 km by the time the enhanced Kelvin wave phase reaches central and eastern Africa (estimates are based on Kelvin convection in Figs. 2 and 3). The cause of such phase speed and zonal-scale changes requires further investigation and is left for future study.

To further illustrate the mean evolution and spatial structure of the Kelvin waves, the regressed 850-hPa geopotential height and winds are presented in Fig. 3. At day 0 (Fig. 3c), the enhanced convection, associated with westerly anomalies, is located over a wide area centered on the base point. Suppressed convection is seen to the west over the eastern Atlantic and coastal West Africa and to the east over the Ethiopian highlands. Zonal wind anomalies are roughly in phase with geopotential anomalies and peak on the equator, consistent with the linear shallow-water Kelvin wave solutions on an equatorial $\beta$ plane (Matsuno 1966) and past observational studies (e.g., WKW00; SK02).

The enhanced convection moves coherently between the eastern Atlantic and eastern Africa between day $-4$ and day $+2$, and by day $+2$ it is centered over the Ethiopian highlands (near 10°N, 40°E; Fig. 3). Throughout this period, the low-level westerlies and southwesterlies are seen to the west and near the enhanced convection, while easterly anomalies dominate the region of suppressed convection, consistent with previously observed convectively coupled Kelvin wave structures over other regions (e.g., WKW00). The low-level wind convergence is slightly to the east of the peak convection, a feature of an eastward-moving convectively coupled wave (SK02). Also, note that the Kelvin convection in Figs. 2 and 3d,e does not have a coherent transition between eastern Africa and the Indian Ocean. The region over eastern Kenya and Somalia is dominated by mean low-level divergence (linked to the Somali jet) and is climatologically dry during the boreal summer season. We expect that a lack of moisture, a result of the divergent flow, inhibits convective development there.

The convective and dynamical structures continue to propagate eastward and are seen over the Indian Ocean at day 4 (Fig. 3e). Figure 3 also shows that Kelvin wave convection peaks north of the equator over the regions between the Pacific and eastern Africa, while it tends to be located closer to the equator over the Indian Ocean, consistent with the geographic distribution of peak Kelvin wave activity shown in Fig. 1.

As indicated in past studies cited in the introduction, when a Kelvin wave approaches a region, its impact is a strengthening of cloud development that yields increased rainfall. The mechanism for increasing cloudiness may be through increasing low-level zonal moisture flux, as suggested by Matthews (2004, his schematic Fig. 10) and Mounier et al. (2008). To highlight this aspect, both the zonal and meridional moisture flux divergence are regressed onto the base point Kelvin-filtered $T_B$ times series used above. Because monsoon flow over Africa is shallow and water vapor is concentrated in the lowest layers of the troposphere [from the surface to 850 hPa; see Cadet and Nnoli (1987), and references therein], the 925-hPa level is chosen.

Figure 4 shows the evolution of the regressed moisture flux divergences (the sum of the zonal and meridional moisture flux divergences) between day $-2$ and day $+2$, the period when the Kelvin wave propagates across tropical Africa. It is clearly seen that the enhanced convection is flanked by moisture flux divergence to the west and convergence to the east. Moisture flux convergence leads convection, an important aspect of the eastward-moving wave signature (e.g., WKW00). Note that even though the theoretical solution of equatorial Kelvin waves requires a zero meridional wind perturbation (Matsuno 1966), the meridional wind anomalies observed here are nonzero but very weak. This may be viewed as part of the response to the off-equatorial convection during this time of the year.

The composites examined above clearly show a coherent structure of a convectively coupled Kelvin wave, consistent with past studies (e.g., SK02; Mounier et al. 2007). Although, from the statistical perspective, com-

[1] Because a phase speed of $\sim$24 m s$^{-1}$ is on the high end of the typical observed range of Kelvin wave phase speeds (e.g., SK03a; SK03b; WKW00), a sensitivity test based on the Kelvin-filtered $T_B$ at 10°N, 10°W in West Africa was performed. Results based on this base point (not shown) confirm that the wave structure and phase speed changes are very similar to that seen in Fig. 2, except that the Kelvin convective amplitudes for this case over central and east Africa are smaller.

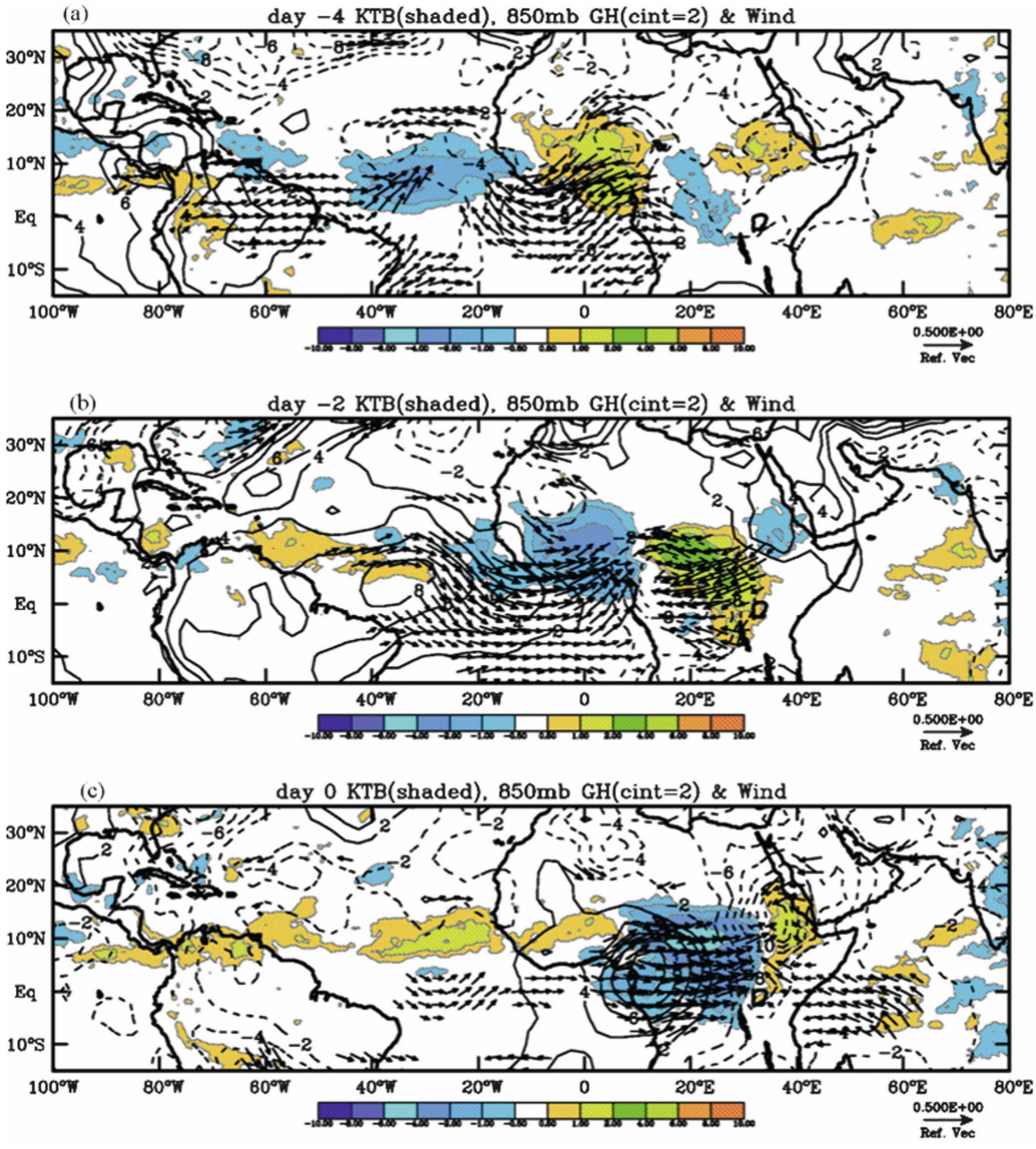


FIG. 3. Regressed $T_B$ (shaded, K), regressed geopotential height, and winds at 850 hPa. Geopotential heights are contoured every 2 gpm. Vectors are drawn if zonal winds are significant at 95% or better (reference wind of 0.5 m s$^{-1}$). The reference point for regression is 10°N, 20°E.

posite Kelvin waves observed over central Africa appear to start over the central and eastern Pacific, it is possible that the wave sources for different cases vary between the central Pacific and central Atlantic. Below, we consider an objective analysis to identify the source regions of Kelvin waves that reach Africa and briefly discuss the mechanisms associated with their initiation.

### c. *Source regions*

As a first step toward identifying the source regions, we distinguish each propagating wave by a phase line, locating the starting and ending points, based on Hovmöller diagrams of Kelvin-filtered $T_B$ (not shown). The phase lines are objectively identified using the following criteria:

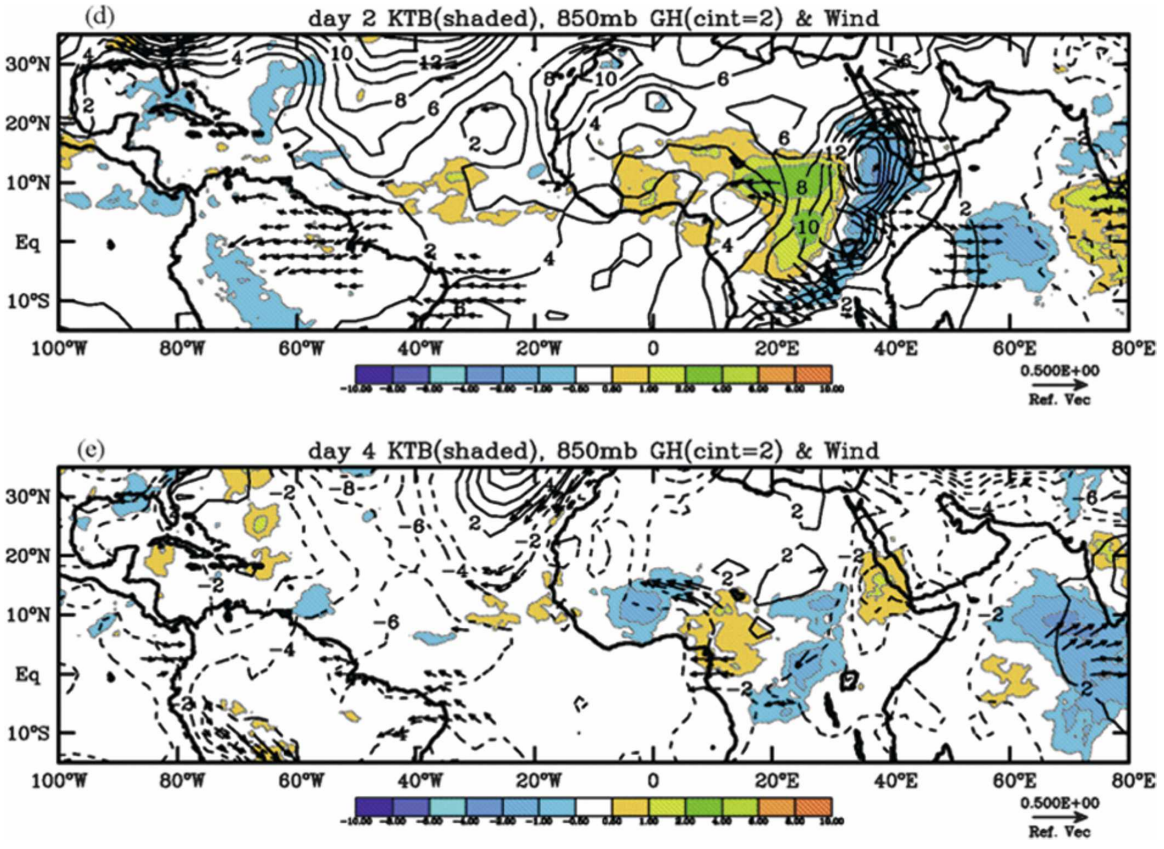


FIG. 3. (*Continued*)

- the convective anomaly should be less than −5 K (a threshold greater than one standard deviation of the Kelvin variance over central Africa; see Fig. 1),
- the wave must propagate for at least 4 days, and
- there must be a continuous propagation for at least 5000 km.

These criteria filter out weaker, short-lived, and less coherent events and limit potentially spurious signals from being counted. This objective identification is performed in a wide area between the central Pacific and the eastern Indian–western Pacific sector (180°–120°E). The latitudinal range is 7°–12°N (a region of maximum Kelvin wave activity; Fig. 1). Then, counts are binned in a 10°-longitude-wide region. The results are shown in Fig. 5.

The result indicates that Kelvin waves can start anywhere in the range of longitudes considered. The primary region of high initiation is the eastern Pacific and western Atlantic (130°–70°W), and a secondary peak is over the eastern Atlantic and coastal West Africa (35°–10°W). A third peak over the Indian Ocean is also observed, but this is not relevant to Kelvin waves over Africa (cf. Fig. 2). As also seen in Fig. 5, the enhanced initiation of Kelvin waves tend to coincide with regions of climatologically enhanced convection (as indicated by lower mean $T_B$).

The objective criteria above do not capture the initial weaker stages of the waves. Some of the waves that are seen over coastal West Africa, for example, may have started out farther to the west (over the eastern Pacific and western Atlantic). To check the stability of the statistics, we lowered the anomaly threshold to −2.5 K (half the standard deviation) and repeated the analysis. The locations for the primary (130°–70°W) and secondary (35°–10°W) regions of initiation were unchanged, but the numbers of events increased.

It should be noted that many of the Kelvin waves initiated over the central and east Pacific weaken over the central Atlantic (a region characterized by higher $T_B$ in Fig. 5), making it difficult for an objective analysis to track them all of the way to Africa. Inspection of Hovmöller diagrams for JAS 1984–2004 indicates that most of the Kelvin wave events initiated over the eastern Pacific (Fig. 5) do indeed reach Africa, despite the weakening of their signals over the Atlantic. Thus, to-

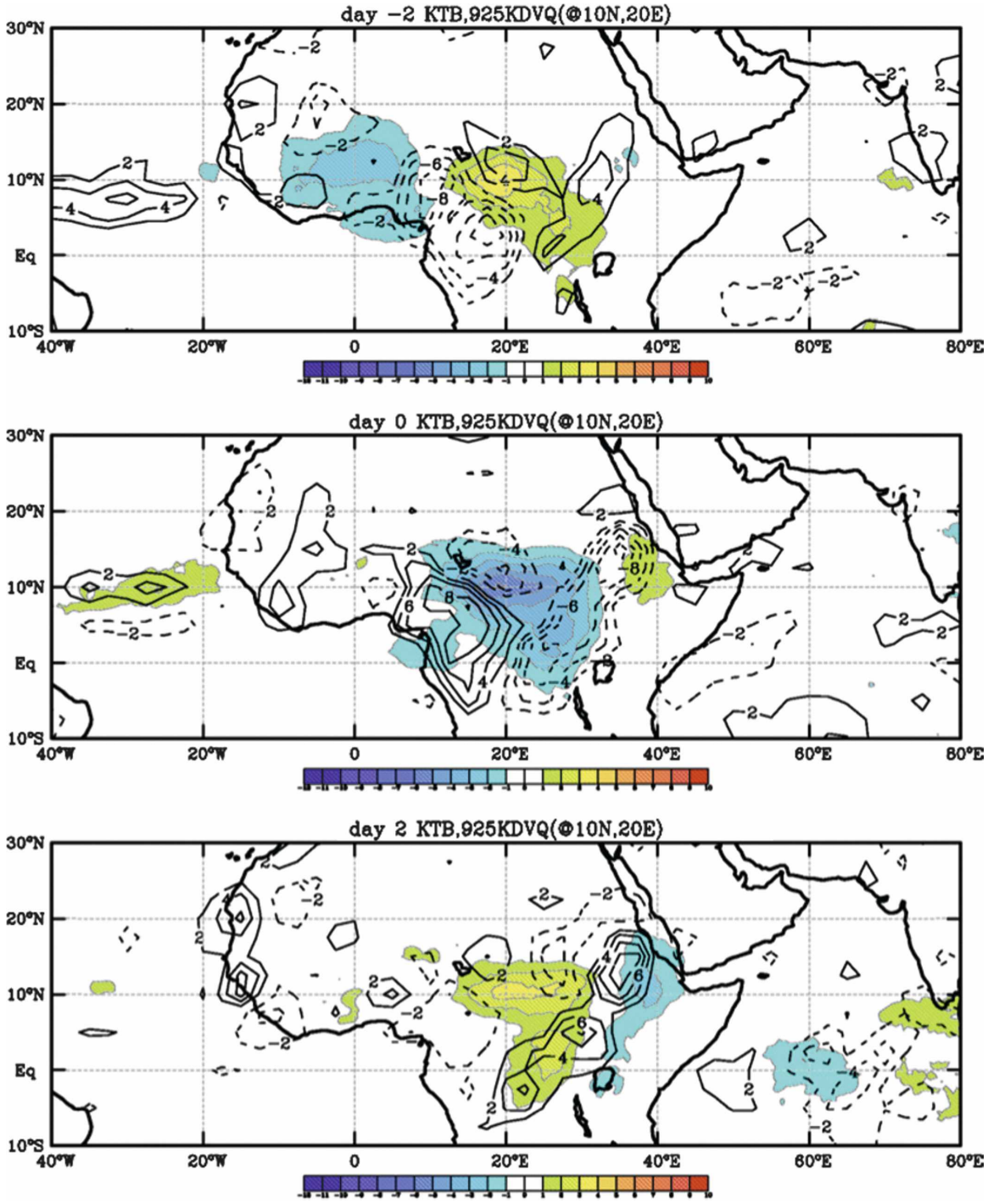


FIG. 4. Regressed $T_B$ (shaded) and regressed moisture flux divergence/convergence (contoured every $2 \times 10^{-6}$ s$^{-1}$ g kg$^{-1}$) between day −2 and day +2. Moisture flux divergence is computed using $[\partial(uq)/\partial x + \partial(vq)/\partial y]$, where $u$ is the zonal wind, $v$ is the meridional wind, and $q$ is the specific humidity. Moisture flux convergence is denoted by dashed lines and divergence is denoted by solid lines. Regressions are performed using a base point time series at 10°N, 20°E.

gether with the evidence shown in Fig. 2, the primary region of Kelvin wave initiation over eastern Pacific and western Atlantic is relevant to the Kelvin waves observed over Africa.

The Kelvin wave initiations may be associated with other wave modes [e.g., the Madden–Julian oscillation (MJO)] or extratropical forcing (e.g., SK03a). The mechanisms associated with initiation of Kelvin waves

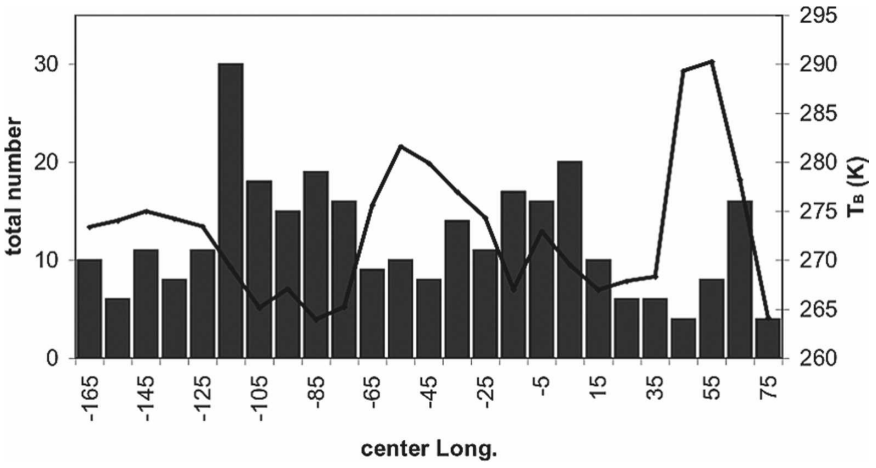


FIG. 5. The histogram of Kelvin convection (bar graph) that originates in a 10°-wide region over the tropical regions and mean $T_B$ (solid line). The ordinates show (left) the total count of Kelvin $T_B$ initiations for JAS 1984–2004 and (right) mean $T_B$ indices (K) for each 10° box. The abscissa shows the center longitudes for each of the 10°-wide regions between 170° and 80°E; the latitudinal band is 7°–12°N. The Kelvin convective anomaly must be $\leq -5$ K and waves must propagate for at least 4 days and for 5000 km from the origin (see text for details).

have been discussed in previous studies. SK03a and SK03b demonstrated that synoptic-scale Kelvin waves that propagate through the central and eastern Pacific were preferentially initiated in association with the active phase of the MJO over the western Pacific. Below, we briefly examine the relationship between the initiation of Kelvin waves and the MJO.

Space–time filtering in the MJO range (with periods of 30–96 days, and eastward wavenumbers of 0–9) has been performed and an MJO-filtered $T_B$ time series at 10°–15°N, 125°–105°W was constructed as a basis for linear regression. This is a region of maximum MJO variance in the eastern Pacific basin (see, e.g., WK99, their Fig. 7d) and also a source region of coherent Kelvin waves observed over Africa (Figs. 2 and 5). Then, each of the global total $T_B$ and global Kelvin wave variance (the square of Kelvin-filtered values at each grid point) were projected onto this reference time series. The results (Fig. 6) indicate that the regressed Kelvin wave activity over the tropical Atlantic and Africa peaks 5–6 days after the peak in MJO convection over the eastern Pacific, suggesting a role for the MJO in triggering Kelvin wave activity, consistent with SK03a. The anomalies shown in the figure are statistically significant, but they are smaller compared with those shown by SK03a. These differences are expected because the base point chosen in SK03a is a region of the western Pacific where MJO variance is generally stronger (see also WK99; Roundy and Frank 2004).

The results and discussion above show that coherent Kelvin wave events can be initiated in association with an MJO event over the eastern Pacific. However, it is also important to note that the eastern Pacific region is characterized by deep convective activity during the boreal summer (Fig. 5). It is likely that even in the absence of the MJO or other dynamic triggers, such as extratropical wave trains (e.g., SK03a), Kelvin waves can still be triggered from in situ deep convection (Fig. 5).

The composite analysis above shows the characteristic features of convectively coupled Kelvin waves that propagate and reach tropical Africa during the boreal summer. We now expand the investigation to consider the interannual variability of Kelvin wave activity, including its relationship with African rainfall and global SSTs.

## 4. Interannual variability

Over tropical Africa, during July–September, the percentage ratio of the standard deviation of the Kelvin wave to the standard deviation of the convective variance in the period of less than 30-days time scale (excluding MJO and lower-frequency variances) is ~20% (not shown). Although the contribution is small on average, it is important to assess how this varies from year to year.

### *a. Observed Kelvin wave variability and its relationship with rainfall*

Figure 7 shows the number of Kelvin wave events that started west of 10°E and propagated through tropi-

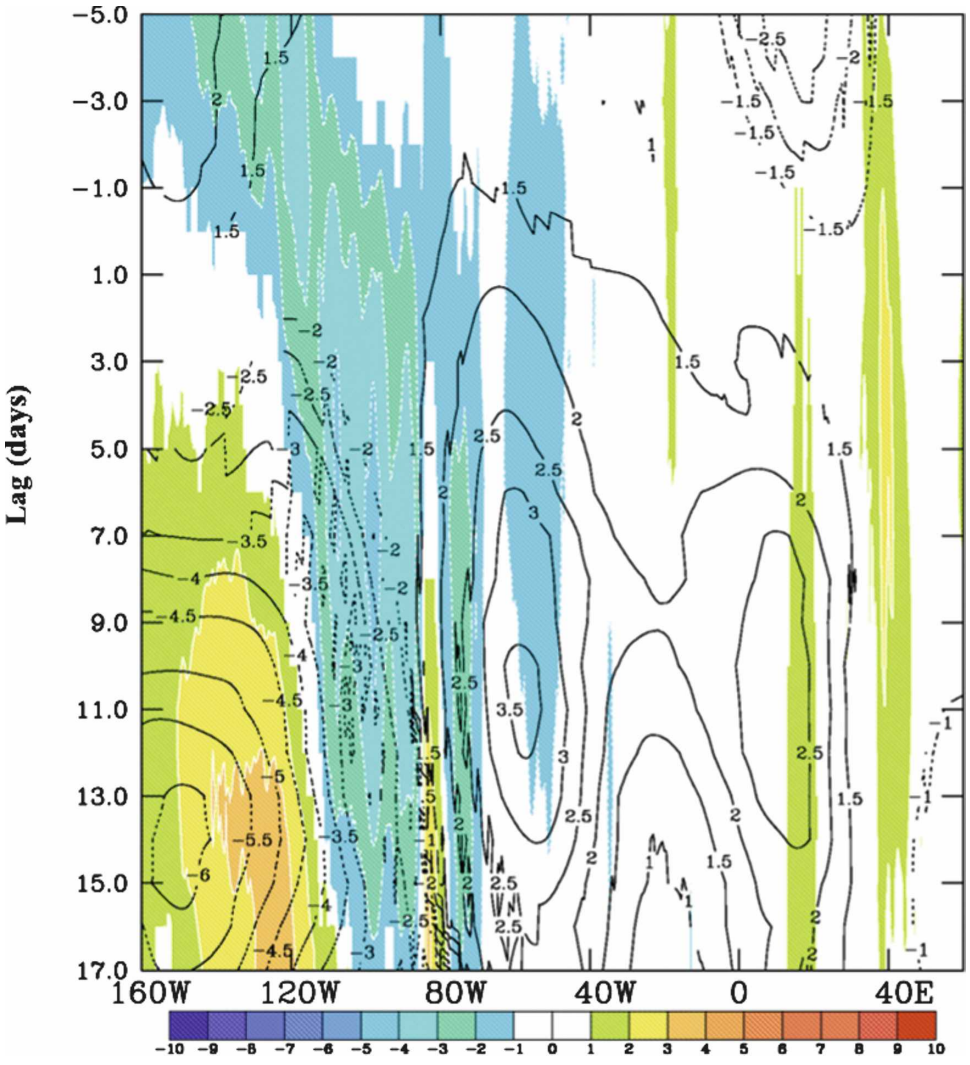


FIG. 6. $T_B$ (shaded, K) and Kelvin-filtered $T_B$ variance (contoured every 0.5 $K^2$) projected onto MJO-filtered $T_B$ at 10°–15°N, 125°–105°W (averaged in a 10°–12°N latitudinal band).

cal Africa east of 20°E (a region of peak Kelvin wave activity, Fig. 1). On average, five–six waves per year propagate into the region, but the interannual variability is large. The most active years were 1984 and 2004, with nine Kelvin wave events, compared with 1992, when just one event occurred according to our criteria. Below, we illustrate how the Kelvin wave variability relates to rainfall.

The Kelvin-filtered $T_B$ variance peaks in the region of 7.5°–12.5°N, 10°–30°E within central and eastern Africa (Fig. 1), and this box is chosen for further illustration of the interannual variability, including amplitude information that is missing in Fig. 7 (see Fig. 8). Anomalously high Kelvin wave variances were observed in 1987, 1990, 1997, and 2004, while anomalously low variances were seen in 1992, 1994, and 1995. Also included in Fig. 8 is rainfall from CMAP for the same region. It may be somewhat surprising to note that high variances occurred during drier-than-average years, while low variances are associated with wetter-than-average years (correlation = −0.38). This is in contrast to the AEW activity over the same area, which is positively correlated with rainfall (correlation = 0.35, not shown). Analysis of the relationship between Kelvin wave activity and SSTs, below, reveals why this is the case.

### b. *The relationship between Kelvin wave variability and global sea surface temperatures*

Figure 9a shows the correlation between global Kelvin $T_B$ variances and the "Niño-3" equatorial

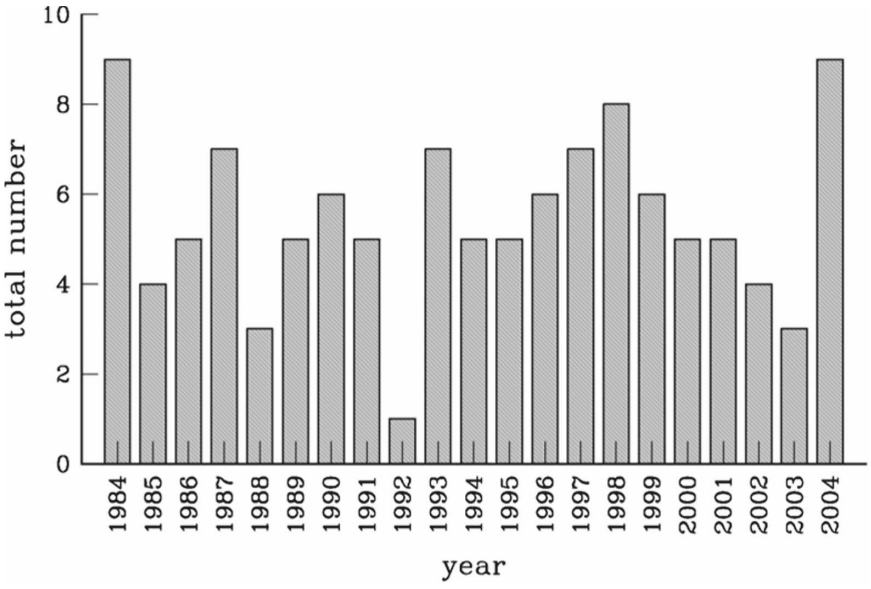


FIG. 7. The year-to-year variability of Kelvin waves that start west of 10°E and that propagated through tropical Africa east of 20°E. Each of the waves must propagate for more than 4 days and are greater than 5000 km (averaged in 7°–12°N).

Pacific SST index (averaged over 5°S–5°N, 150°–90°W). The basis for choosing the Niño-3 SST index is related to the fact that it has a significant relationship with the tropical North African summer rainfall (e.g., Ward 1998; Rowell 2001). A highly significant positive correlation (>0.8) is seen over the eastern Pacific region, indicating an important impact of the SSTs on Kelvin wave activity there. The simplest explanation of this result is that warming of SSTs over the eastern Pacific is associated with an increase in local convection, and this in turn may induce more Kelvin wave activity to the east. The Kelvin wave activity over Africa is also positively correlated with the remote SSTs (correlation >0.4), suggesting that variability in the convectively active source region is related to the variability of the Kelvin wave activity over Africa. Consistent with this, the highest Kelvin variance over central and east Africa was observed in 1987 and 1997, coinciding with the warmest Niño-3 SSTs (Fig. 10). Further inspection of Fig. 10 indicates that the weakest Kelvin wave variances over the same region occurred in 1992, 1994, and 1995, when the Niño-3 SST was colder than average.

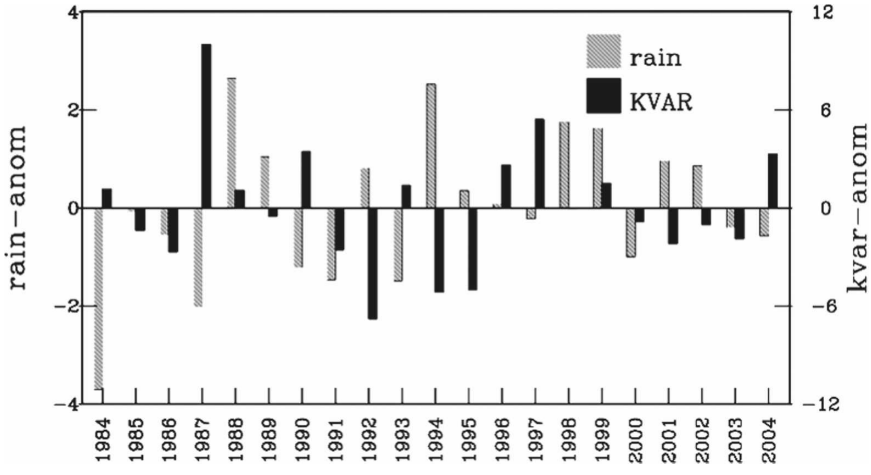


FIG. 8. The interannual variability of Kelvin-filtered $T_B$ variance (dark shaded, $K^2$) and rainfall (light shaded) anomalies (mm $day^{-1}$) at 7.5°–12.5°N, 10°–30°E.

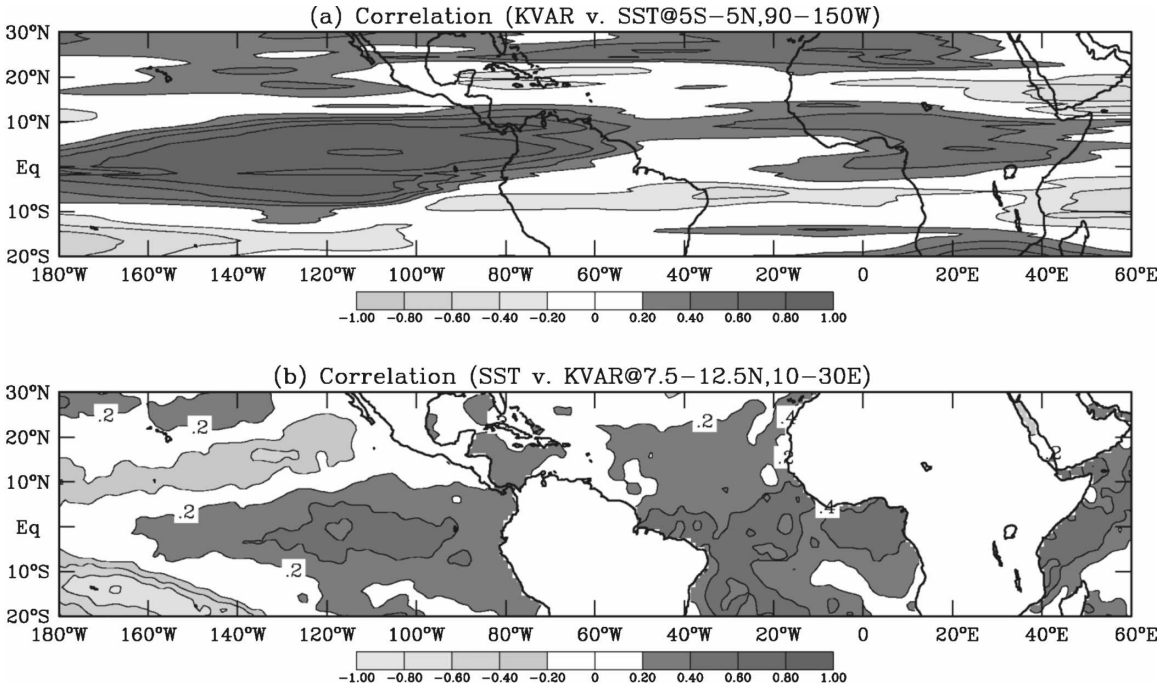


FIG. 9. (a) The correlation between global Kelvin-filtered $T_B$ variance and sea surface temperature at Niño-3 (5°S–5°N, 150°–90°W), and (b) the correlation between global sea surface temperature and Kelvin-filtered $T_B$ variance at 7.5°–12.5°N, 10°–30°E. (Positive correlations are dark shaded and negative correlations are light shaded.)

However, this simple relationship is not always observed. For example, in 1988, the Kelvin wave activity was slightly above average, when the Niño-3 SST was the coldest, suggesting the potentially important role of other source regions (such as warm SSTs over the western Atlantic; not shown).

Figure 9b shows the correlation between the Kelvin wave activity over Africa (at 7.5°–12.5°N, 10°–30°E) and global SSTs. Again, consistent with Fig. 9a, a relatively strong correlation (>0.4) is seen over the equatorial eastern Pacific. Positive correlations (>0.4) are also seen over the equatorial Atlantic and the Gulf of Guinea. The in-phase relationship with the warming of SSTs over the equatorial Atlantic suggests a favorable background environment for convectively coupled Kelvin wave propagation. As shown in previous studies

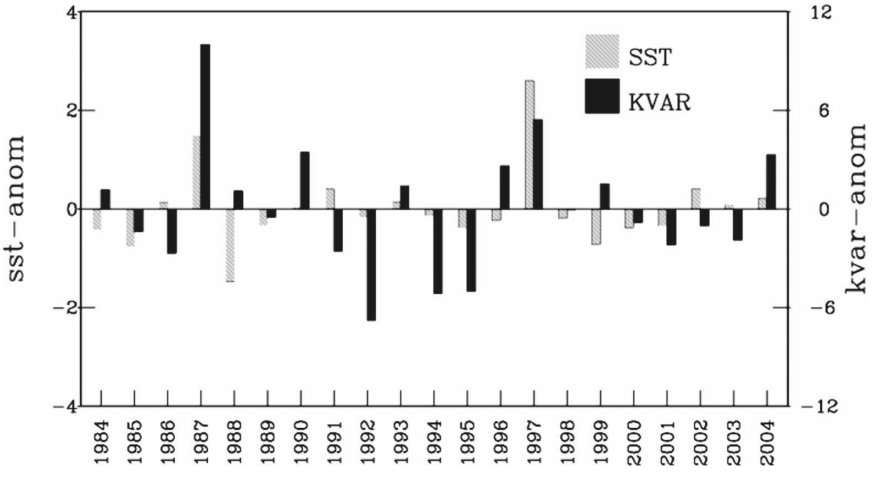


FIG. 10. As in Fig. 8, but for Niño-3 SST anomaly (light shaded, K) and Kelvin-filtered $T_B$ variance (dark shaded, $K^2$).

(e.g., Ward 1998), increased SSTs in the Gulf of Guinea also result in a weaker temperature gradient between the land surface and the sea, a signature of a weaker monsoon and reduced rainfall in the region.

Our analysis shows that increased SSTs over the eastern equatorial Pacific is related to increased Kelvin wave initiation there. It is well known that warming of the equatorial east Pacific is often associated with dry years over tropical Africa (e.g., Ward 1998; Rowell 2001). A warm eastern equatorial Pacific favors more Kelvin wave initiations, but at the same time it suppresses rainfall over tropical Africa via a more slowly varying teleconnection and associated subsidence (e.g., Ward 1998; Rowell 2001; Janicot et al. 2001). Thus, together with the equatorial Atlantic SST, this might help explain the negative correlation found between Kelvin wave activity and rainfall over Africa (Fig. 8).

Thus far, the results and discussion have focused on composite structures of Kelvin waves that propagate across Africa. Results above also indicate that while Kelvin waves are not the most important synoptic weather events during wet years in the region, they can be relatively more important during the dry years. The section below highlights the impact of a Kelvin wave on convection and daily rainfall over tropical Africa. This provides an opportunity to investigate how this mean composite signal compares with individual weather events.

## 5. Impact of an intense Kelvin wave event on convection and rainfall

Here, a strong Kelvin wave event that occurred during JAS 1987, an active Kelvin wave year over Africa (Fig. 8), is chosen for further analysis. This was also one of the most active periods of eastward-propagating convective structures observed in Mekonnen et al. (2006, their Fig. 14).

Figure 11 is a Hovmöller diagram of unfiltered $T_B$ and Kelvin-filtered $T_B$ for JAS 1987 and for the region between the date line and 120°E (averaged between 7° and 12°N). Convective activity occupies a much larger area over the eastern Pacific basin, while it occupies a relatively smaller area over the Atlantic and tropical Africa. The convective activity over the Pacific–western Atlantic sector is composed of several MCSs. While the large-scale envelope displays eastward propagation, associated with Kelvin wave activity, the smaller-scale MCSs show a clear westward propagation (e.g., SK02; SK03a).

Also seen in Fig. 11 are about six coherent Kelvin wave events that start over the Pacific and propagate across tropical Africa. The Kelvin wave events that propagated across Africa during 1–10 and 14–20 September were initiated in association with the active phase of the MJO (not shown), consistent with results in Fig. 6. However, the Kelvin wave events during 10–15 July and 6–12 August were formed in association with deep convection over the Pacific.

We now examine the intense Kelvin wave event that impacted tropical Africa during 6–12 August (this event is identified by arrows in Fig. 11). This wave started over the eastern Pacific around 29 July and propagated eastward and decayed over the Southeast Asia–western Pacific region, near 120°E, around 18 August. This wave traveled about 24 000 km, with an average phase speed of about 13 m s$^{-1}$. Further inspection of this Kelvin wave shows that its phase speed was high over the Pacific and Atlantic, slows down over Africa (~11 m s$^{-1}$), and increase when it leaves Africa, consistent with the composite result seen in Fig. 2. Below, we offer a brief description of the synoptic situation during the period when the Kelvin wave propagated across tropical Africa, and we explore the extent to which the wave impacted convective development and rainfall there.

Figure 12 shows the Kelvin wave and associated convection as it propagated across tropical Africa. The Kelvin wave reached coastal West Africa on 7 August and was associated with enhanced convection around the coast and Guinea highlands. By 9 August, the Kelvin wave is seen over the region between 0° and 10°E in West Africa. The Kelvin wave continued to move eastward and by 11 August it is observed over the region between eastern Sudan and the central Ethiopian highlands. Throughout this time, the Kelvin wave was associated with convective activity. Note that the locations of peak Kelvin wave convection seen here are consistent with the locations of peak Kelvin wave anomalies shown in Fig. 3.

To highlight how the Kelvin wave impacted daily rainfall, we consider the rainfall and Kelvin wave indices from three regions following the wave propagation. These regions are coastal West Africa, representing the Guinea highlands and eastern Senegal (10°–15°N, 15°–10°W; R1), a region composed of Togo–Benin and western Nigeria (7°–12°N, 0°–5°E; R2), and a region in East Africa (7°–9°N, 35°–40°E; R3). Figure 13 shows the average daily rainfall and Kelvin wave index for the three locations. When the enhanced phase of the Kelvin wave approached coastal West Africa (R1) on 6 and 7 August, rainfall over the region abruptly increased from about 5 to about 20 mm day$^{-1}$. Rainfall significantly decreased to less than 5 mm day$^{-1}$ in the following days, after the Kelvin wave phase had passed the region.

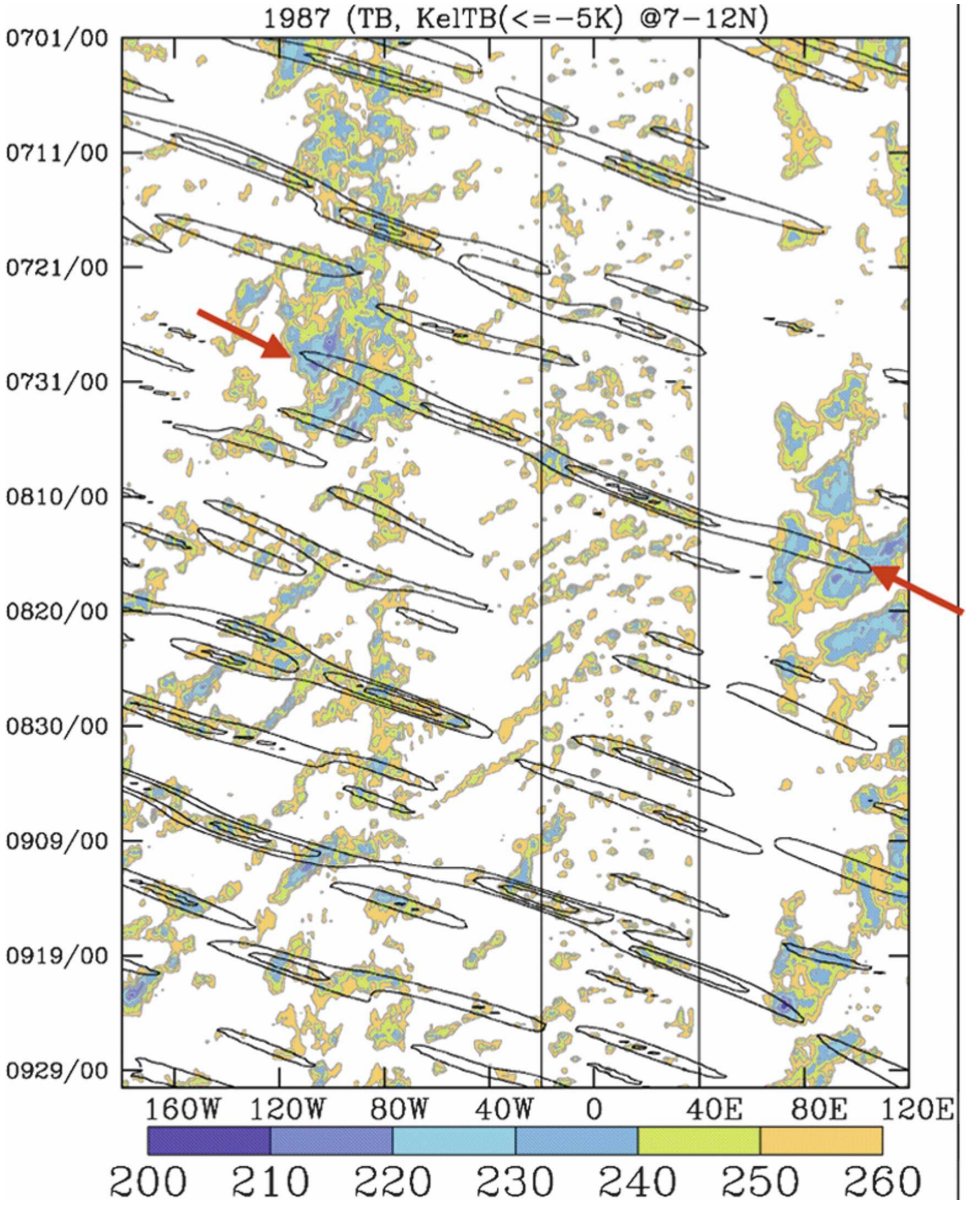


FIG. 11. Time–longitude Hovmöller of convection (represented by $T_B < 260$ K; shaded) and Kelvin-filtered $T_B$ (contoured every 5 K from −5 K; only enhanced and strong phases of Kelvin convection are shown for clarity) for JAS 1987 (averaged in 7°–12°N latitudinal band). Vertical lines at 20°W and 40°E show, respectively, coastal West Africa and eastern African highlands. The red bold arrows identify the strongest Kelvin wave phase that propagated through Africa between 6 and 12 Aug 1987.

A significant increase in rainfall, from about 5 to more than 12 mm day$^{-1}$, was also observed on 8 August over R2 in West Africa, associated with the enhanced Kelvin wave. Rainfall sharply fell to about 3 mm day$^{-1}$ on 9 August after the Kelvin wave phase had passed the region. The rainfall increase on 10 August was not related to Kelvin wave activity, an indication of other forcing mechanisms. Similarly, when the enhanced Kelvin convection approached the Ethiopian highlands (R3) on 10 and 11 August, the rainfall increased from about 6 to about 12 mm day$^{-1}$ (Fig. 13c). The rainfall significantly dropped to ~1 mm day$^{-1}$ on 12 August after the passage of the enhanced Kelvin wave.

To check whether the abrupt rainfall increase over West and East Africa could also be associated with westward-moving wave disturbances, we examined the evolution of the AEWs over the selected regions (not shown). In general, the AEWs were either very weak or

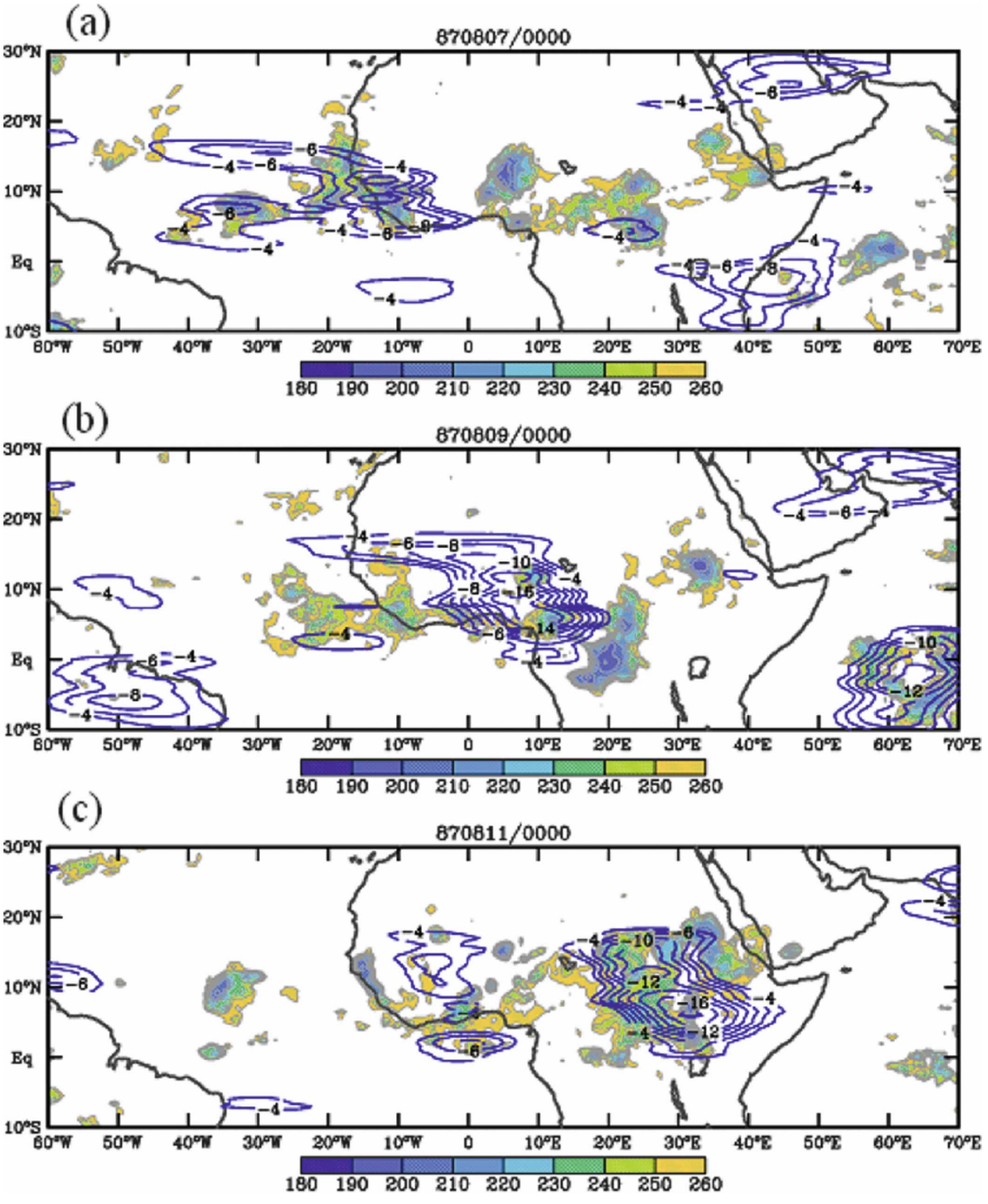


FIG. 12. (a)–(c) Synoptic maps of Kelvin-filtered $T_B$ (contoured every 2 K; only the enhanced phase is shown for clarity) and unfiltered $T_B$ (shaded; $< 260$ K) every 2 days between 7 and 11 Aug 1987.

did not correspond well with the daily rainfall samples. This suggests that the Kelvin wave activity during this period was more important for increased rainfall and convective enhancement than the AEWs. Indeed, prior to the Kelvin wave passage, the AEW activity was very weak during this particular event. It was not until the Kelvin wave had passed that the AEW activity became significant.

Thus, we suggest that, at least occasionally, Kelvin waves play a role in the initiation of AEWs via enhanc-

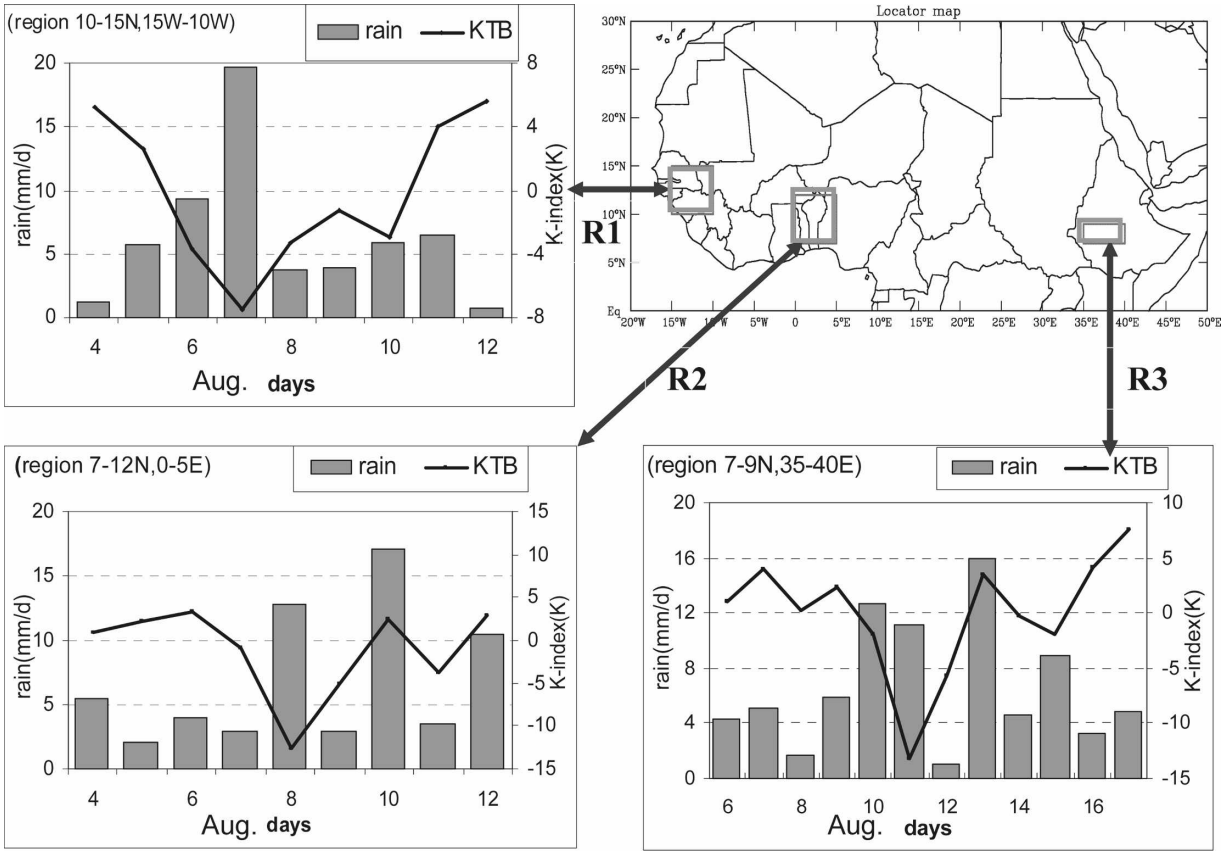


FIG. 13. Daily rainfall (shaded, mm day$^{-1}$) and Kelvin wave indices (solid lines, K) for R1 (Guinea and eastern Senegal), R2 (Togo–Benin and western Nigeria), and R3 (Ethiopia) in tropical Africa. The rainfall for the two West African boxes (R1 and R2) is extracted from the IRD archive, while the East African box (R3) consists of eight rainfall stations from Ethiopia.

ing convective triggers over Africa, consistent with the triggering ideas promoted in recent studies (e.g., Mekonnen et al. 2006; Kiladis et al. 2006; Hall et al. 2006; Thorncroft et al. 2008). Figure 14 shows enhanced Kelvin wave and AEW phases for August 1987. Four of the five AEWs start over Africa in association with the passage of the enhanced phase of the Kelvin wave. One of the AEWs (denoted as "#2") appears to exist prior to the Kelvin wave, but intensified after interacting with the enhanced Kelvin wave phase. These AEWs can also be seen to propagate across the Atlantic and, for some of them, into the Pacific.

While it appears that several AEWs in August 1987 were formed in association with the passage of this Kelvin wave, analysis of other years indicates that this is not such a common event. Indeed, a cursory look at the Hovmöller diagrams of JAS 1984–2004 of Kelvin-filtered $T_B$ and AEWs shows that, on average, about three AEWs per year are formed in association with convection enhanced by the Kelvin wave activity (accounting for ~10%, assuming ~30 AEWs per year; Berry et al. 2007).

## 6. Summary and final comments

This study has highlighted the structure and variability of convectively coupled Kelvin waves that impact sub-Saharan Africa during the boreal summer. The origin of these Kelvin waves can be traced as far back as the eastern Pacific and western Atlantic. Results show that Kelvin convection over Africa during the monsoon season is peaked north of the equator, while the dynamical fields tend to be symmetric with respect to the equator, consistent with Mounier et al. (2007) and with Kelvin wave structures seen in other parts of the tropics (WKW00; SK02; SK03a; SK03b).

Composite analysis using a regression technique shows that the phase speed and wave periodicity change as the Kelvin waves propagate between the Pacific–Atlantic sector and tropical Africa. These waves propagate faster over the Pacific–western Atlantic sector (~25 m s$^{-1}$), slow down over tropical Africa (~14 m s$^{-1}$), and propagate faster as they exit Africa. The wave periodicity also changes from about 8 days over the eastern Pacific and the Atlantic to about 4 days

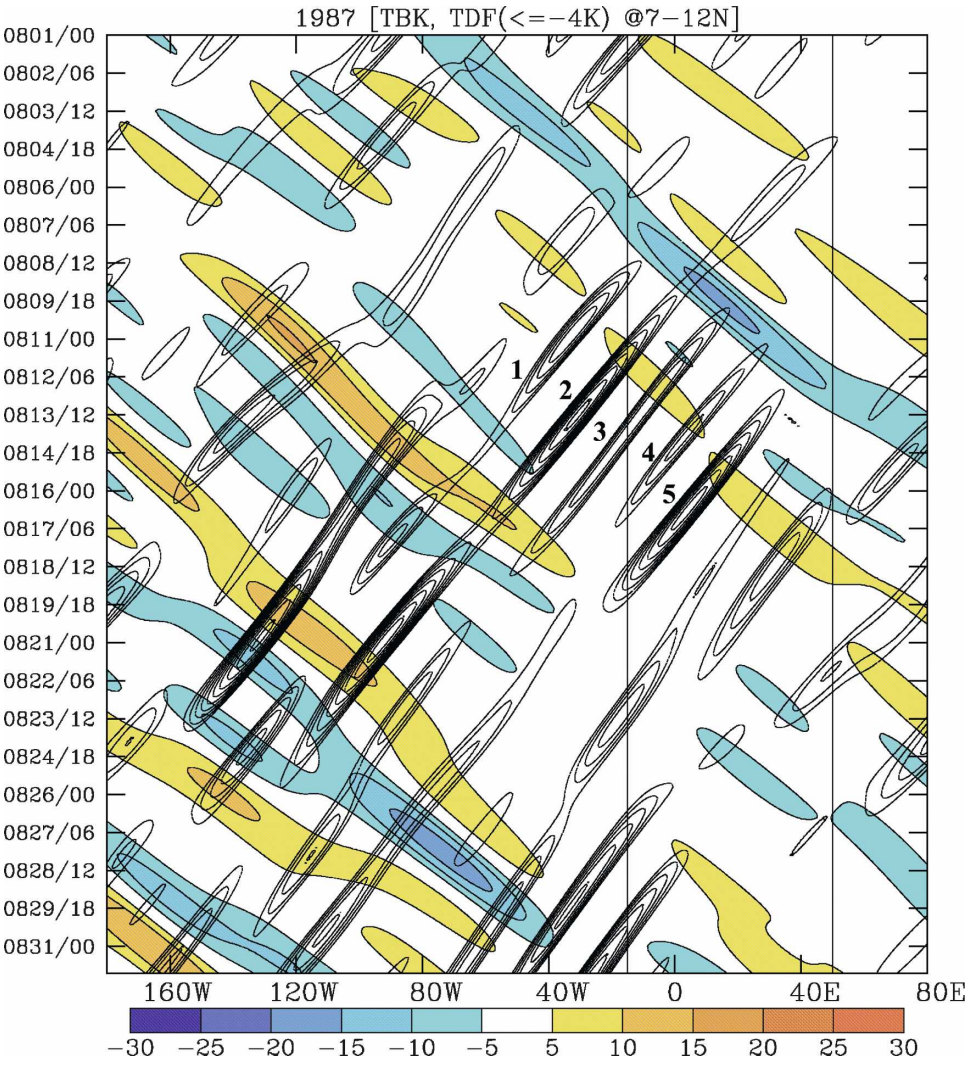


FIG. 14. Kelvin-filtered $T_B$ (shaded and contoured as shown) and AEWs (contoured every 2 K from −4 K; only negatives shown for clarity) for August 1987, averaged between the 7° and 12°N latitudinal range. AEW activity was determined by filtering $T_B$ in the period of 2–7.5 days with westward wavenumber of 6–20 [the "tropical disturbance (TD)-filtered" domain], which effectively captures easterly waves during the northern summer (see Kiladis et al. 2006). Weak and potentially spurious signals are suppressed, and only significant phases of both Kelvin waves and AEWs are displayed (i.e., magnitudes that correspond to more than one standard deviation). Numbers 1–5 denote the AEWs initiated or enhanced in association with the enhanced phase of the Kelvin wave. Vertical lines at 20°W and 50°E show the west and eastern limits of tropical Africa, respectively.

over central and eastern Africa. Consistent with this, the zonal scale of the Kelvin wave decreases as it reaches tropical Africa.

The Kelvin wave activity over tropical Africa exhibits large interannual variability. Our analysis has shown that anomalously high Kelvin wave activity tends to occur during dry years over Africa, while low activity occurs during wet years. The Kelvin wave variability is positively correlated with SST anomalies in the equatorial east Pacific. The simple interpretation is that warming of the SSTs leads to increased local convection, which can cause increased Kelvin wave initiation over the source region. The same SST anomalies that are favorable for enhanced Kelvin wave activity are likely to be responsible for the dry years over Africa (Ward 1998; Rowell 2001; Janicot et al. 2001), explaining the fact that active Kelvin wave years tend to be dry years over the region.

Composite analyses have been compared with an intense Kelvin wave event in August 1987. The daily rain-

fall rates associated with the intense Kelvin convection in the three regions across tropical Africa increased to about 10, 20, and 12 mm day$^{-1}$, which is more than double the previous day's values. The rainfall then fell sharply to less than 5 mm day$^{-1}$ when the wave moved past the regions. This is consistent with past studies that show the association between Kelvin waves and increased convective organization and daily rainfall over the Pacific (SK02; SK03a; Sobel et al. 2004; Takayabu and Murakami 1991).

Along with Mounier et al. (2007, 2008), this study highlighted the fact that although less dominant than the westward-moving African easterly waves, convectively coupled Kelvin waves can indeed influence tropical African rainfall during the boreal summer. Researchers and forecasters concerned with the synoptic variability of rainfall over this region during this time of the year should be aware of the potential impact of Kelvin waves, especially in dry years when their relative importance appears to be increased. Also, the fact that most of these Kelvin waves propagate through Africa into the Indian Ocean raises the intriguing possibility that processes operating over tropical Africa may influence the nature and predictability of convection in the equatorial Indian Ocean (e.g., Roundy 2008).

*Acknowledgments.* This research was supported by a grant from the National Science Foundation (ATM: 0507976). CLAUS data are obtained from the British Atmospheric Data Centre (online at http://badc.nerc.ac.uk/cgi-bin/data_browser/data_browser/badc/claus/). The ERA-40 data are obtained from the ECMWF data server (online at http://www.ecmwf.int). Rainfall data for Ethiopian stations is acquired from the Ethiopian Meteorological Services Agency, Addis Ababa, Ethiopia. The CMAP data are available at CPC/NOAA (online at http://www.cpc.ncep.noaa.gov/products/global_precip/html/wpage.cmap.html). We thank Dr. Paul Roundy of the University at Albany, Albany, NY, for useful discussion and Dr. Kevin Hodges of the Reading University, Reading, United Kingdom, for his help in reformatting the CLAUS data. We thank three anonymous reviewers for their useful comments, which greatly improved the manuscript.

## REFERENCES

Berry, G., C. Thorncroft, and T. Hewson, 2007: African easterly waves—Analysis using objective techniques. *Mon. Wea. Rev.,* **135,** 1251–1267.

Cadet, D. L., and N. O. Nnoli, 1987: Water vapour transport over Africa and the Atlantic Ocean during summer 1979. *Quart. J. Roy. Meteor. Soc.,* **113,** 581–602.

Hall, N. M. J., G. N. Kiladis, and C. D. Thorncroft, 2006: Three-dimensional structure and dynamics of African easterly waves. Part II: Dynamical modes. *J. Atmos. Sci.,* **63,** 2231–2245.

Hodges, K. I., D. W. Chappell, G. J. Robinson, and G. Yang, 2000: An improved algorithm for generating global window brightness temperatures from multiple satellite infrared imagery. *J. Atmos. Oceanic Technol.,* **17,** 1296–1312.

Janicot, S., S. Trzaska, and I. Poccard, 2001: Summer Sahel-ENSO teleconnection and decadal time scale SST variations. *Climate Dyn.,* **18,** 303–320.

Kiladis, G. N., C. D. Thorncroft, and N. M. J. Hall, 2006: Three dimensional-structure and dynamics of African easterly waves. Part I: Observations. *J. Atmos. Sci.,* **63,** 2212–2230.

Matsuno, T., 1966: Quasi-geostrophic motions in the equatorial area. *J. Meteor. Soc. Japan,* **44,** 25–43.

Matthews, A. J., 2004: Intraseasonal variability over tropical Africa during the northern summer. *J. Climate,* **17,** 2427–2440.

Mekonnen, A., 2006: The role of Kelvin wave activity on convection and rainfall over tropical Africa. Preprints, *27th Conf. on Hurricanes and Tropical Meteorology,* Monterey, CA, Amer. Meteor. Soc., 4D.2. [Available online at http://ams.confex.com/ams/pdfpapers/108508.pdf.]

——, C. D. Thorncroft, and A. R. Aiyyer, 2006: Analysis of convection and its association with African easterly waves. *J. Climate,* **19,** 5405–5421.

Mounier, F., G. N. Kiladis, and S. Janicot, 2007: Analysis of the dominant mode of convectively coupled Kelvin waves in the West African monsoon. *J. Climate,* **20,** 1487–1503.

——, S. Janicot, and G. N. Kiladis, 2008: The West African monsoon dynamics. Part III: The quasi-biweekly zonal dipole. *J. Climate,* **21,** 1911–1928.

Nguyen, T. T. H., and J. P. Duvel, 2008: Synoptic wave perturbations and convective systems over equatorial Africa. *J. Climate,* **21,** 6372–6388.

Rayner, N. A., D. E. Parker, E. B. Horton, C. K. Folland, L. V. Alexander, D. P. Rowell, E. C. Kent, and A. Kaplan, 2003: Global analyses of sea surface temperature, sea ice, and night marine air temperature since the late nineteenth century. *J. Geophys. Res.,* **108,** 4407, doi:10.1029/2002JD002670.

Reed, R. J., D. C. Norquist, and E. E. Recker, 1977: The structure and properties of African wave disturbances as observed during Phase III of GATE. *Mon. Wea. Rev.,* **105,** 317–333.

Roundy, P. E., 2008: Analysis of convectively coupled Kelvin waves in the Indian Ocean MJO. *J. Atmos. Sci.,* **65,** 1342–1359.

——, and W. M. Frank, 2004: A climatology of waves in equatorial region. *J. Atmos. Sci.,* **61,** 2105–2132.

Rowell, D. P., 2001: Teleconnections between the tropical Pacific and the Sahel. *Quart. J. Roy. Meteor. Soc.,* **127,** 1683–1706.

Sobel, A. H., S. E. Yuter, C. S. Bretherton, and G. N. Kiladis, 2004: Large-scale meteorology and deep convection during TRMM KWAJEX. *Mon. Wea. Rev.,* **132,** 422–444.

Straub, K. H., and G. N. Kiladis, 2002: Observations of a convectively coupled Kelvin wave in the eastern Pacific ITCZ. *J. Atmos. Sci.,* **59,** 30–53.

——, and ——, 2003a: Extratropical forcing of convectively coupled Kelvin waves during austral summer. *J. Atmos. Sci.,* **60,** 526–543.

——, and ——, 2003b: Interaction between the boreal summer intraseasonal oscillation and higher-frequency tropical wave activity. *Mon. Wea. Rev.,* **131,** 945–960.

Takayabu, Y. N., 1994: Large-scale disturbances associated with

equatorial waves. Part I: Spectral features of the cloud disturbances. *J. Meteor. Soc. Japan,* **72,** 433–448.

——, and M. Murakami, 1991: The structure of super cloud clusters observed in 1-20 June 1986 and their relationship to easterly waves. *J. Meteor. Soc. Japan,* **69,** 105–125.

Thorncroft, C. D., N. M. J. Hall, and G. N. Kiladis, 2008: Three-dimensional structure and dynamics of African easterly waves. Part III: Genesis. *J. Atmos. Sci.,* **65,** 3596–3607.

Tompkins, A. M., A. Diongue, D. J. Parker, and C. D. Thorncroft, 2005: The African easterly jet in the ECMWF integrated forecast system: 4DVar analysis. *Quart. J. Roy. Meteor. Soc.,* **131,** 2861–2885.

Wang, H., and R. Fu, 2007: The influence of Amazon rainfall on the Atlantic ITCZ through convectively coupled Kelvin waves. *J. Climate,* **20,** 1118–1201.

Ward, M. N., 1998: Diagnosis and short-lead term prediction of summer rainfall in tropical North Africa at the interannual and multidecadal timescales. *J. Climate,* **11,** 3167–3191.

Wheeler, M., and G. N. Kiladis, 1999: Convectively coupled equatorial waves: Analysis of clouds and temperature in the wavenumber–frequency domain. *J. Atmos. Sci.,* **56,** 374–399.

——, ——, and P. J. Webster, 2000: Large-scale dynamical fields associated with convectively coupled equatorial waves. *J. Atmos. Sci.,* **57,** 613–640.

Xie, P., and P. A. Arkin, 1997: Global precipitation: A 17-year monthly analysis based on gauge observations, satellite estimates and numerical model outputs. *Bull. Amer. Meteor. Soc.,* **78,** 2539–2558.

Yang, G., and J. Slingo, 2001: The diurnal cycle in the tropics. *Mon. Wea. Rev.,* **129,** 784–801.